J Mater Sci (2007) 42:9284–9292
DOI 10.1007/s10853-007-1892-3

The microstructure and mechanical properties of Fe–Cu materials fabricated by pressure-less-shaping of nanocrystalline powders

Rosa Di Maggio · Gloria Ischia · Mauro Bortolotti · Federico Rossi · Alberto Molinari

Received: 23 November 2006 / Accepted: 29 May 2007 / Published online: 27 July 2007
© Springer Science+Business Media, LLC 2007

Abstract The microstructure of Fe-40%$_{wt}$Cu nanocrystalline powders, prepared by mechanical alloying, was studied before and after the consolidation process. Pressure-less-shaping (PS) was used to consolidate the powders. The PS technique, similar to metal injection moulding (MIM), does not require external pressure in order to fill up the mould. The key factor of the process of consolidation is the use as binder a hybrid inorganic–organic monomer, formed by the reaction of zirconium propoxide and 2-hydroxy ethyl methacrylate. This type of monomer, mixed with the metallic powders, formed slurry having low viscosity, which was easily poured into mould. The binder stiffened upon polymerization. Some pieces were produced through debinding and sintering, both performed under inert atmosphere in order to avoid metal oxidation. Different microstructure and density were observed depending on the maximum sintering temperatures, ranging from 904 to 1,120 °C. In the sample sintered at 1,120 °C, the crystalline domains of the copper phase were of about 40 nm.

Introduction

One of the most relevant aspects of nanotechnology is the forming process. Powder Metallurgy (PM) could be exploited for the production of small-medium size pieces. At the aim to facilitate the retention of nanostructures, high pressure had better to be used in the consolidation of nanocrystalline metallic powders [1]. Among the processes of powders consolidation, metal injection moulding (MIM) is one of the most important net-shape techniques, though the fabrication of large samples requires increasingly complex apparatuses. Furthermore, it cannot be neglected that MIM is quite expensive owing to the costs of feedstock injection systems, steel moulds and long debinding processes [2, 3]. An alternative way is pressure-less-shaping (PS). It is a less expensive process, since injection and steel moulds are replaced by casting and polypropylene, respectively. PS was successfully applied to consolidation of D2 and AISI 316 L steel powders, as described in a previous study [4]. In this study, PS was applied to the consolidation of a nanocrystalline iron–copper alloy. The binder used for PS consolidation is a hybrid inorganic–organic thermosetting monomer [5, 6]. The hybrid monomer was able to wet powders and form fluid slurry.

The Fe–Cu alloy is one of the most investigated systems, because copper significantly improves mechanical properties of iron compacts [7–15]. However, the conventional sintering process of Fe–Cu powders was found critical, due to the expansion caused by copper penetration into iron grain boundaries of particles above 1,083 °C, the Cu melting point. The expansion was not observed when the powders were coated by copper or consolidated using injection moulding [7–10]. It was also observed that the expansion was reduced by the presence of carbon [11].

For this study, mechanically alloyed Fe-40%$_{wt}$Cu powders were consolidated using PS. The particles showed irregular morphology and surface oxides. After the consolidation, some specimens were subjected to thermal debinding and then sintered at different temperatures. The thermal decomposition of the binder leaves zirconium

R. Di Maggio (✉) · G. Ischia · M. Bortolotti · F. Rossi · A. Molinari
Department of Materials Engineering and Industrial Technologies, University of Trento, Via Mesiano 77, Trento 38100, Italy
e-mail: rosa.dimaggio@ing.unitn.it

oxide, supposed homogenously distributed into the metallic matrix. Accordingly, a strengthening and a pinning effect in metallic grain growth were expected. The effects of preparation parameters and temperature sintering on the microstructure and hardness of the pieces were investigated. Although the high temperatures make the nanocrystallinity of the copper and iron grains be hardly retained, it will report below some interesting results about the sample sintered at 1,120 °C.

Experimental procedure

Materials and sample preparation

MECHANOMADE® S101 Fe-40%$_{wt}$Cu powder was produced by M.B.N. s.r.l., through a mechanical alloying process. The size distribution is broad, ranging from 5 to 150 μm. The tap density of the powder is 4.9 g/cm^3, whereas 8.27 g/cm^3 is the powder density measured by pycnometer.

The binder used for this study consisted of hybrid monomer having the following general formula: $Zr(OPr^n)_{4-x-y}(acac)_x(HEMA)_y$. It was obtained by mixing *n*-propoxide of zirconium ($Zr(OPr^n)_4$), acetylacetone (acacH) and 2-hydroxyethylmethacrylate (HEMA) in the molar ratio of 1/0.55/4, respectively. Benzoyl peroxide (BPO) (2%wt of the HEMA amount) was added to the metallic powder. All the reagents (Aldrich) were pure graded and used without any purification. The powder and the liquid binder were mixed at room temperature. The slurry was then poured into polymeric moulds. Teflon, silicone and polypropylene were the best materials for moulds because of their low adhesion to the binder. The binder polymerized without heating within a few minutes. In order to increase the cross-linking, a thermal curing was performed at 80 °C. Then the compacts underwent to debinding process and the following thermal multi-step treatment assured the most reliable results:

- 20 → 190 °C at 3 °C/min in Ar-5%H_2;
- 30 min at 190 °C in Ar-5%H_2;
- 190 → 240 °C at 1.5 °C/min in Ar-5%H_2;
- 30 min at 240 °C in N_2-10%O_2;
- 30 min at 240 °C in Ar-5%H_2;
- 240 → 355 °C at 1 °C/min in Ar-5%H_2;
- 40 min at 355 °C in Ar-5%H_2.

The sintering was isothermally carried out for 1 h in a vacuum (5×10^{-4}–7×10^{-5} mbar), using a tubular furnace. A small part of copper could evaporate from the outer surface of specimens, due to high vacuum. The heating rate was 5.5 °C/min. The maximum temperatures of the isothermal step were 940, 1,050, 1,080, 1,090, 1,100, 1,115 and 1,120 °C.

Instrumentation

The viscosity of the slurries was measured by means of the torsion viscometer (VISCOLOG). TMA/SS6000 (SEIKO INSTRUMENTS) was used to perform Thermo-Mechanical Analysis (TMA). Thermal Gravimetric Analyses (TGA) and Dynamic Mechanical Thermal Analyses (DMTA) were performed using HT-DSC/TGA (SETARAM) and DMS6100 (SEIKO INSTRUMENTS), respectively. The samples were heated at 1 °C/min until 500 °C in air or argon or argon-hydrogen. High Temperature HT 1800 Plus furnace (Linn) was used, coupled with a turbomolecular pump (LH Leybold), in order to achieve high vacuum. The densities of the consolidated samples were determined using the buoyancy method applying the Archimedes Principle (sample weight measurements in air and in water).

X-Ray diffraction (XRD) analysis was carried out using an imaging plate (IP) diffractometer (ItalStructures IPD3000) in pure reflection geometry, equipped with a copper anode X-ray tube, a silicon multilayer monochromator (k-α1) on the incident beam and a nickel filter system on the diffracted beam. The imaging plate acquisition system (Perkin–Elmer Cyclone) was operated at 600 dpi collecting a 20–120° 2θ range for each sample. A full profile Rietveld refinement was performed using the MAUD (Materials Analysis Using Diffraction) software [16]; the refined quantities were the volume fraction and lattice parameters of each crystallographic phase, as well as crystallite size and r.m.s. (root mean square) microstrain of the Fe and Cu phases, reported in Table 1. The isotropic model reported in [17] was used for the microstructural analysis. The full-profile refinement procedure, combined with a wide 2-dimensional IP detector system, was found to be an improved tool for microstructure analysis, as compared to traditional detector and single peak procedures. Moreover, this procedure minimized the statistical errors caused by heterogeneity of samples.

Transmission Electron Microscope (TEM) Phillips 400T operated at 120 kV was used for observing the Fe-40%$_{wt}$Cu powder and the specimens sintered at 1,120 °C. The powder was ultrasonically suspended in alcohol and then spread onto a copper grid covered with an amorphous carbon film. As concerns bulk materials, thin discs were prepared from 0.5 mm thick foils. The discs were mechanical polished on both sides and reduced to the thickness of 100 μm. Then, a 3 mm diameter disc was punched and milled by argon ions in a DuoMill Gatan apparatus, with an accelerating voltage of 6 kV and a current of 1 mA.

The Energy Dispersive X-ray Spectra (EDXS) were acquired through the FALCON X-ray detector for preparing chemical composition maps of selected regions of the

Table 1 Density, crystallite size and average volume shrinkage of the Fe–Cu powder and some sintered specimens

Samples/sintering temperature (°C)	Mechanomade® Fe-40%Cu powder	940	1,050	1,080	1,090	1,100	1,115	1,120
Density (g/cm^3)	4.9[a]	6.1	6.3	6.6	6.9	7.1	7.5	7.6
Relative density (%)[b]	59.3	74.2	76.4	80.5	83.5	86.6	91.5	95.1
Fe grain size (nm)	35 (±4)	83 (±9)	–	86 (±6)	120 (±16)	–	–	210 (±25)
Cu grain size (nm)	45 (±8)	80 (±17)	–	81 (±6)	48 (±2)	–	–	39 (±4)
Fe r.m.s. microstrain	15.89E-4 (±0.29E-4)	25.89E-4 (±0.45E-4)	–	6.95E-4 (±0.64E-4)	30.56E-4 (±0.53E-4)	–	–	18.58E-4 (±0.51E-4)
Cu r.m.s. microstrain	15.51E-4 (±0.48E-4)	29.53E-4 (±0.72E-4)	–	10.30E-4 (±0.24E-4)	0 (–)	–	–	0 (–)

[a] Tap density of the powder

[b] 8.27 g/cm^3 is the powder pycnometer density

samples, observed by Environmental Scanning Electron Microscope (ESEM) (Philips XL30 ESEM-TMP).

The hardness measurement was based on the Oliver & Pharr method through the indentation method using CSM Instruments Nano-Hardness Tester (NHT) with trigonal pyramid indenter tip [18, 19]. The flat surface of the specimens, polished by 0.5 μm diamond paste, was chemically attacked by a nital 2% solution before the hardness measurement, in order to perceive different phases by the optical microscope attached to tester and indent them apart. The hardness values reported in Table 2 were averaged from 4 to 5 indentations on any given sample.

Flexural tests were performed on small rectangular samples (12 × 3×1 mm) in a three points configuration, by using Seiko EXSTAR TMA/SS6100 Thermal Mechanical Analyser. In order to obtain modulus of elasticity in bending, flexural stress and strain in the outer surface (%) of samples were measured.

Results and discussion

The starting powder contains two phases: Fe and Cu. The phases have grain size of 35 and 45 nm, respectively. These values are greater to those reported in literature and in the range of 10–20 nm [14, 20]. In the XRD spectrum, the peaks of FCC copper phase were shifted slightly, so that the amount of the Fe–Cu solid solution was low. Moreover, the weight fraction of the two phases, as obtained with Rietveld quantitative analysis, corresponded nearly to the nominal elemental composition: a large presence of metastable Fe–Cu solid solution was thus excluded [20]. Accordingly, the mechanical alloying in the powders was supposed to be not appreciable, probably due to the poor intense and/or short milling. He and Ma reported that a single FCC phase, a metastable supersaturated solid solution, was only present in 20 h ball-milled $Cu_{40}Fe_{60}$ powder [20]. Indeed, Fe and Cu have similar atomic size, so that the shift with respect those of FCC Cu phase is slight even for a complete solid solution. The same authors showed that the single FCC phase transformed back to nearly pure elemental phases after annealing at 600 °C, below the temperature used in the present study for sintering. Indeed, the spontaneous decomposition of solid solution upon heating during consolidation can be used to produce in situ two nanophase composites [20].

The size of the Fe–Cu crystallites was measured, during the TEM observations, less than 50 nm, in a good agreement with XRD results. The Selected Area Electron Diffraction (SAED), not here reported, showed the presence of copper, iron and also Cu_2O. This last suggested the powders were oxidized. Moreover, the SAED showed diffraction ring consistent with the small size of the Fe crystallites [21].

The Fe–Cu powder flows slightly when dry, due to the irregular morphology of the particles and the high surface area. The amount of binder is one of the most important parameters in order to control the casting step of PS process. Using the mathematical and empirical models developed for MIM, the critical loading of the Fe–Cu powder feedstock was calculated equal to

Table 2 Microhardness of selected samples

	Fe-rich phase microhardness (Hv)	Cu-rich phase microhardness (Hv)
Mechanomade® Fe-40 wt%Cu powder		500 ± 20
Microcrystalline copper specimen		172 ± 15
Sintered at 1,080 °C		215 ± 10
Sintered at 1,120 °C	200 ± 5	245 ± 5

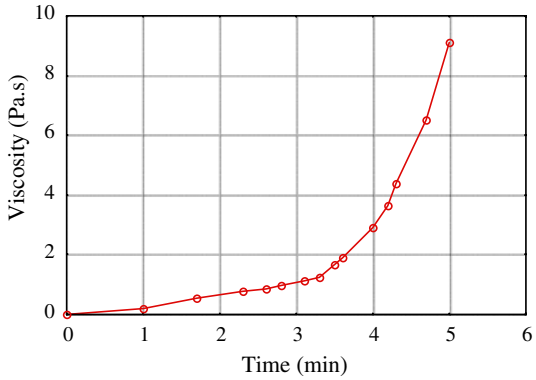

Fig. 1 Viscosity versus time for the mixture powder-hybrid binder with polymerization initiator benzoyl peroxide (BPO)

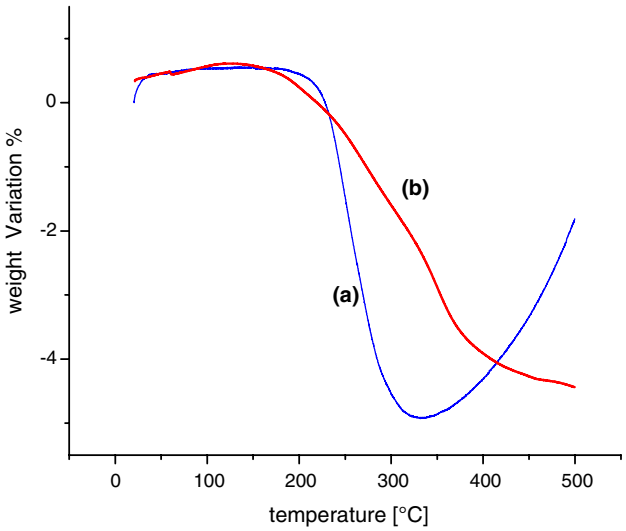

Fig. 2 Thermo-gravimetric analyses (TGA) on green specimens performed at 1 °C/min in (**a**) air and (**b**) argon atmospheres

59.7%$_{vol}$, whereas the actual loading used in the study was 52% [2].

The monomer used as binder is a hybrid inorganic–organic molecule, having both hydrophilic (–OH) and hydrophobic (alkyl or methacrylic groups) functionalities. The ability of the binder to cover the metallic particles was favoured by the presence of the cuprite on the surface of the metallic particles. Indeed, the hydroxyls interacted with the oxide, whereas the hydrophobic groups pointed outward: the metallic particles resulted capped by organic groups. These last caused steric hindrance, making the particles repel each other during the casting of the slurry. This accounted for the fluidity of the resulting feedstock, which showed a very low viscosity (2–10 mPa s) after the preparation. However, the viscosity of the binder increased with time, because hybrid monomer formed oligomers and in a few minutes the polymerization started (Fig. 1). Indeed, at the aim of producing through PS specimens having complex geometry, the mould should be designed with gates or feeding pipes as linear as possible and risers for spilling the excess of the binder. Upon polymerization, the binder became a rigid polymer. The elastic modulus of the fabricated specimens was around 1.5 GPa, as measured by three point flexural test.

The thermal decomposition of the polymer was carried out both in oxidizing or non-oxidizing environment. In the first case, the combustion of the organic residual occurred at temperatures between 250 and 300 °C, accompanied by large CO_2 loss (see TGA in Fig. 2a). Above 300 °C, the binder decomposition was partially masked by the remarkable increase in weight due to the iron oxidation. This drawback was probably favoured by the nanocrystalline nature of the Fe–Cu powder. As a consequence, in the XRD spectrum of the sample after debinding, the peaks of FeO and Fe_3O_4 phases were present (Fig. 3). Moreover, the mass loss of the specimens treated under inert or reducing atmosphere was lower than that recorded in air (see TGA in Fig. 2b). Accordingly, carbonaceous residues remained into the metallic composites, along with traces of zirconium oxide [4]. In a previous study, the presence of carbon was supposed to increase the dihedral angle and lessen the critical expansion occurring in the sintering of Fe–Cu system [11].

The debinding treatment was planned on the basis of the results of the thermal and mechanical analyses, performed on the samples. The TMA curve in Fig. 4 showed that an expansion occurred at about 190 °C. This last was due to the gas of the combustion in air, given that the irregular surface of the particles hindered their flow out. The occurrence of the expansion was also confirmed by DMTA curve, not here reported. This phenomenon caused macroscopic defects. In order to avoid that, the flow of the combustion gas from the core to the surface was slowed down, by using a low heating rate and an isothermal step just below 190 °C. The final debinding treatment was a multi-step process performed under inert atmosphere, with only a short step in air at the aim of reducing the oxidation the metallic particles during the combustion of the organic part of the binder.

The density and the crystallite size of the sintered samples, as a function of the maximum temperature, are reported in Table 1. At 940 °C the grain size and microstrain were about twice those of the metallic powder. This suggests that the continuous growth of the particles and the thermal mismatch during cooling exerted pressure on the lattices. At 1,080 °C, iron and copper phases were intimately mixed along with small copper and zirconia segregation (see Fig. 5a, b). In this sample, both iron and copper crystallites kept nanometric size, meanwhile the microstrain decreased. Moreover, the negligible growth of

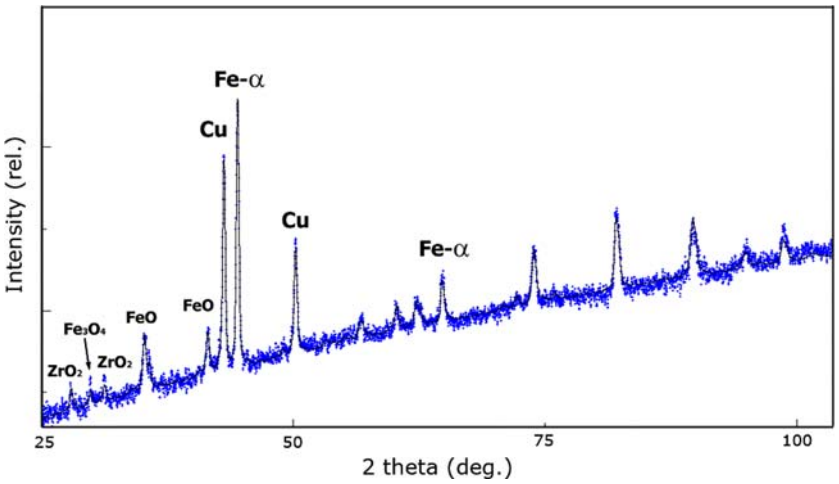

Fig. 3 X-ray diffraction (XRD) spectrum of the surface of a sample after debinding in air

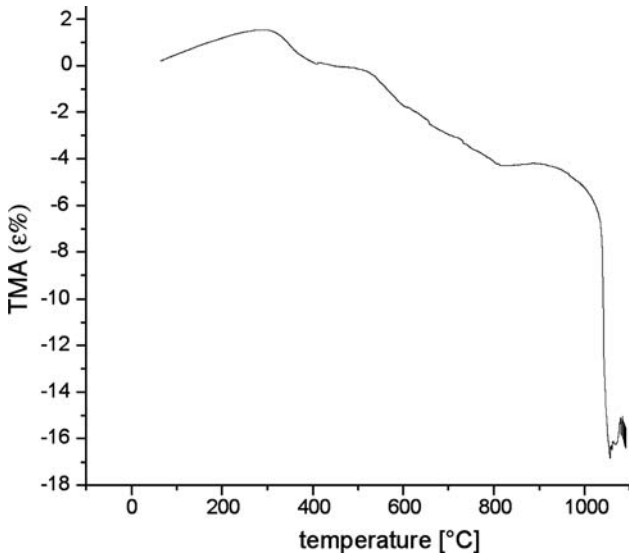

Fig. 4 Thermo-mechanical analysis (TMA) curve of sintering

iron grains was attributable to the pinning effect of zirconia, derived from the binder decomposition. Greater densities were obtained above the melting temperature of copper ($T_{m,\ Cu}$ = 1,083 °C) by liquid phase sintering. Indeed, the highest strain in the Fe grains occurred in specimens sintered at 1,090 °C, due to the greater thermal mismatch between the melted copper and solid phases.

Full density can be achieved at the expense of grain coarsening, as already observed by other authors [1, 22, 23]. The Fe–Cu alloy consisting of a single metastable solid solution was found relevant at the aim of delaying solute segregation and retaining nanoscale grain size [14, 20]. Nevertheless, the sample sintered at 1,120 °C resulted something intermediate. Its bulk density was 95.1% of that theoretical. The data in Table 1 indicate that, although the iron grains coarsened, the sizes of the copper crystalline domains were even decreased with respect the samples sintered at lower temperatures. Moreover the copper grains showed no microstrain at all: the copper was completely melted during sintering and new crystals nucleated upon cooling. Indeed, considering that grain growth in Cu is faster than in Fe, there may be two factors contributing to the prevailing of nucleation against grain growth: a quite fast cooling, even if not a real quenching, and the zirconia pinning effect.

According to the TEM observations, the sample sintered at 1,120 °C showed three different regions: those in which the Selected Area Electron Diffraction (SAED) indicated Fe as the single constituent (Fig. 6a), areas where the SAED indicated Fe–Cu–ZrO_2 (Fig. 6b–d) and Cu–ZrO_2 (Fig. 7a–d). The Fe regions are polycrystalline and the size is estimated lower than 100 nm (see Fig. 6a). The morphology of Fe–Cu–ZrO_2 areas showed a matrix with very small dark spots (Fig. 6c). These spots are ZrO_2 particles dispersed in the matrix, as indicated in the dark field image in Fig. 6d. A picture of the Cu–ZrO_2 zone and the SAED of the same area are reported in Fig. 7a and b, respectively. They showed the presence of ZrO_2 intimately mixed with Cu. Their sizes were ranging from a few nanometers to about 100 nm (Fig. 7c). Accordingly to Fig. 7d, the Cu crystallites sizes in the sintered sample at 1,120 °C were still nanocrystalline. Indeed, Cu crystallites were estimated lower than 50 nm. The formation of mixed regions accounted for the nanometric size of the Cu crystallites, since pinning effect affects in a greater extent Cu-rich phase than Fe one.

The crystallites size does not seem consistent with that from XRD analyses, which provided values greater for both iron and copper crystallites sizes. However, differently from the XRD analysis, which brought about average values, the TEM measurements are relative to the observed areas, so the values were affected by unpredictable changes in the microstructure and composition.

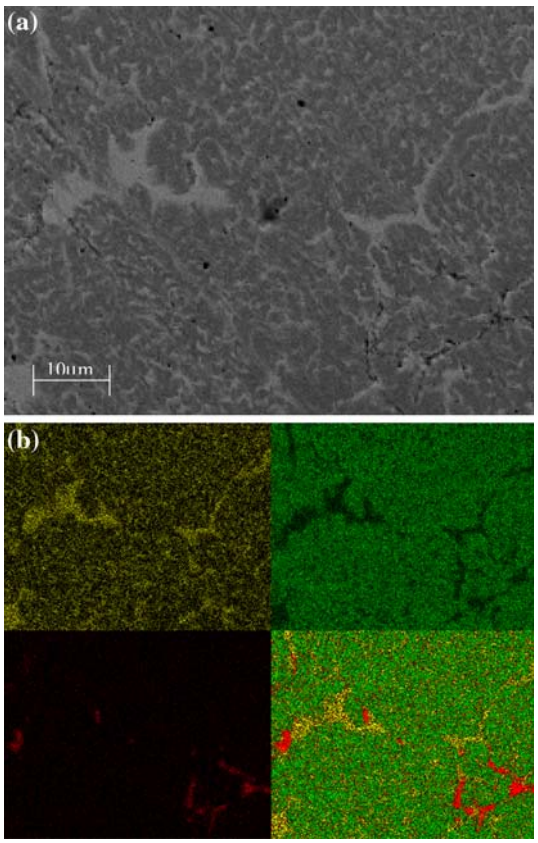

Fig. 5 Environmental scanning electron microscope (ESEM) micrograph (**a**) and chemical elements map (**b**) of a sample sintered at 1,080 °C. *Yellow*, *green* and *red areas* correspond to copper, iron and zirconium, respectively

The results of the hardness measurements are reported in Table 2. The milled Fe–Cu powder particles consist of mixed nanodomains of Fe and Cu. Accordingly, the hardness measurement provided a single very high value, even if lower than that of fully consolidated $Fe_{60}Cu_{40}$ alloy in Ref. 14. Indeed, this is not a surprise, taking into account that in our case grain size is greater. The strain hardening and mostly nanometer-scale grains size of the particles were the two factors contributing to hardness [14, 15, 22–26]. Moreover, this last showed an increase over the rule-of-mixture prediction (about 400 Hv), as calculated in Ref. 14. Indeed, the strengthening enhancement stems from the existence of FCC–BCC boundaries, more effective than same phase grains boundaries in blocking slip transmission across the interfaces, and not from the presence of solid solution, which is negligible as discussed before.

However, the thermal sintering at high temperature of the consolidated specimens necessarily caused grain growth, relaxation of the residual stresses and recovery of the plasticity. Thus, an average value of 215 Hv was recorded for sample sintered at 1,080 °C. Also in this case the coarsening of crystalline grains and even the growth of Cu and Fe phase domains can account for the low value. Given that the grains were still nanocrystalline, the finding is quite unsatisfactory. Actually, the collapse of hardness is mostly due to the large amount of remaining porosity (15%), which is homogeneously distributed into the consolidated specimen as observed by ESEM analysis. A remarkable effect of remaining porosity on hardness value has been already observed for nanocrystalline Fe–29Al–2Cr alloy consolidated by sinterforging [15].

As discussed before, the sintering at 1,120 °C let the segregation of Cu-rich phase be complete: the size of Cu phase (not crystalline grain) was between a few and 10 μm, whereas of that of Fe domain was between 10 and 40 μm. They were anymore nanophase composites, though Cu phase was still nanocrystalline. In Table 2 are shown the hardness values of the two phases, which were obtained by separate tests. They are much different with respect the hardness values of nano- and micro-composites reported in literature [14, 22–26]. The smaller size of copper grains than that of iron can account for the greater hardness of Cu phase. Moreover, as we discussed before the Cu domain is not at all a pure phase, but just a Cu-rich phase, containing iron and especially zirconia. Their presence can explain both the smaller grain growth in Cu, which instead should be much faster than in Fe, and the greater hardness. Moreover, the value of Cu-rich domains for the same reasons is greater than that of micro-crystalline pure copper (172 Hv), as measured with the same indenter apparatus for a comparison, or nanocrystalline sintered composites [14, 22–26]. The Fe-rich phase contains much less zirconia, so that the strengthening effect is averagely lower.

A three point flexural test was performed on the specimen sintered at 1,120 °C and the failure occurred with 2% of plastic deformation. Some dimples and micro-voids were visible on the fracture surface (Fig. 8) and a small ductile contribution to the fracture mechanism was supposed. Figure 9 shows the EDXS analysis performed on the same fracture surface. It consisted mainly of copper. Accordingly, it can be concluded that the failure grew through the copper rich phase, following an inter-granular path. This effect is consistent with the greater hardness of Cu-rich phase, which increased brittleness. However, the copper segregation at the grain boundary makes the failure be less catastrophic than that occurring in presence of metal carbide or sulphide segregations.

Conclusions

Pressure-less-shaping (PS) technique was applied to Fe–Cu nanocrystalline powders for producing composites of small-medium size. The key point of the process consisted of using

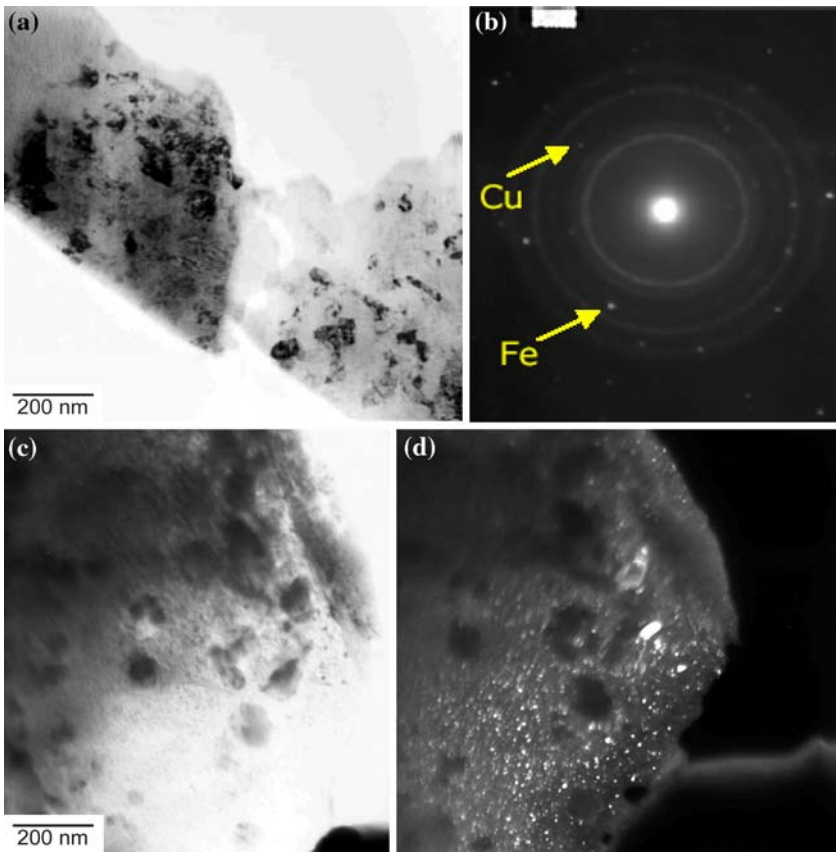

Fig. 6 Sample sintered at 1,120 °C: (**a**) Fe region; (**b**) Selected area electron diffraction (SAED) showing the presence of ZrO_2, with ring spectrum, and some spots of Cu and Fe; (**c**) bright field of a Fe–Cu–ZrO_2 area; (**d**) dark field obtained using a portion of the 1,0,1 ring of ZrO_2

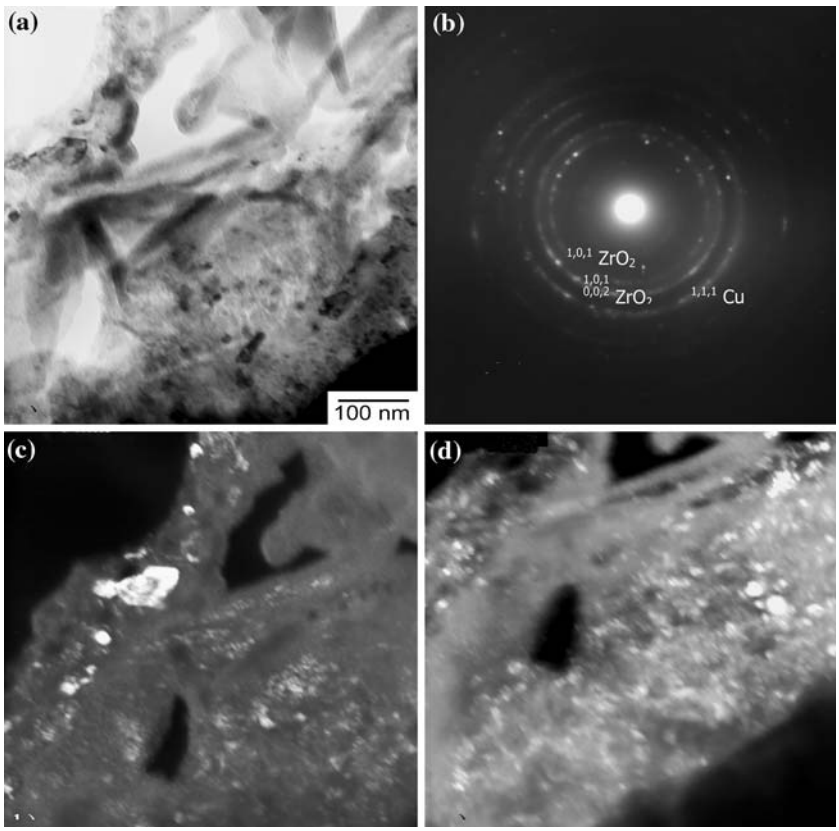

Fig. 7 Sample sintered at 1,120 °C: (**a**) bright field of a Cu–ZrO_2 area; (**b**) selected area electron diffraction (SAED) of the area shown before (ZrO_2 and Cu are indicated); (**c**) dark field obtained using a portion of the 1,0,1 ring of ZrO_2 displayed in the SAED; (**d**) dark field obtained using a portion of the 1,1,1 Cu ring displayed in the SAED

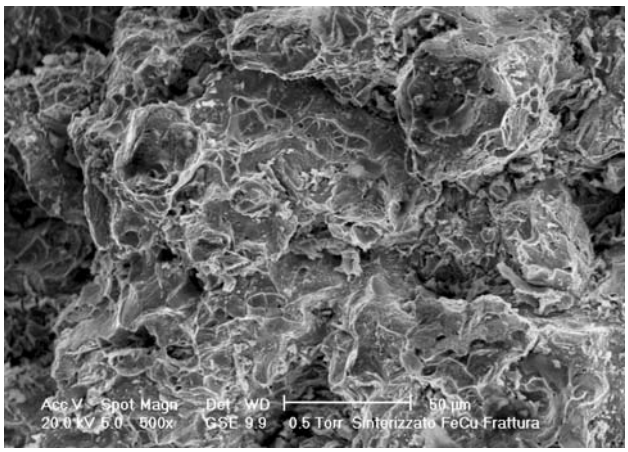

Fig. 8 Environmental Scanning Electron Microscope (ESEM) micrograph of a fracture surface of a specimen sintered at 1,120 °C

a hybrid monomer of general formula $Zr(OPr^n)_{4-x-y}(acac)_x(HEMA)_y$ as binder. This made the viscosity of the slurry be very low, so that no external pressure was required to fill up the moulds. These last may be made of polypropylene. The low viscosity is due to a repulsive effect of alkyl groups of binder, which was attached to metal particles surface by hydroxyl functionalities. Upon polymerization, stiff compacts were obtained by cross-linking of binder. Then, the organic component of the binder was eliminated through a suitable thermal treatment, leaving in the brown body very small amount of zirconia.

The samples sintered below the melting temperature of the copper (1,083 °C) showed low density, but crystalline nanometric size. At higher temperatures, density increases and meantime grain size, even if residual zirconia had a pinning effect on the growth of the metallic crystalline grains. In order to close to full density and meanwhile maintain nanoscale size grains, the specimens had to be sintered at 1,120 °C. At this temperature, the microstructure was quite peculiar, consisting of nanocrystalline copper (about 40 nm) covering iron phase. As observed by TEM analysis, the crystallites size maintained low due to the zirconia and iron, which hindered the nuclei growth of the copper.

Hardness measurements indicate a strengthening effect due to nanometric grain and phase sizes only for the Cu–Fe powders, attributed to interphase boundaries between different structures. The sintered specimens are softer than powders because of the residual porosity and coarsening of both grain and domain sizes. At 1,120 °C, the enlargement of the two phases was so enhanced that hardness could be measured separately: iron phase was softer than copper, which is harder than other micro and nanocrystalline Cu materials. This features also the fracture behaviour of composite, which exhibited an appreciable ductility.

PS confirmed to be a useful technique to consolidate Cu–Fe powders. Since every thermal treatment causes grain coarsening, the debinding and sintering processes should be properly fit, when nanoscale grain and domain

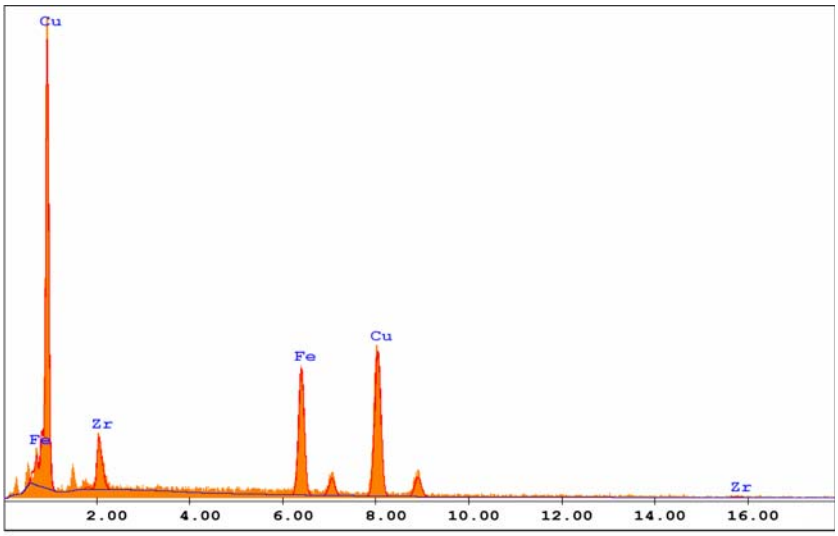

EDAX ZAF Quantification (Standardless)
Element Normalized
SEC Table : Default

Element	Wt %	At %	K-Ratio	Z	A	F
FeK	29.87	33.14	0.3355	1.0201	0.9745	1.1300
CuK	64.92	63.31	0.6002	0.9947	0.9295	1.0000
ZrK	5.22	3.54	0.0471	0.9255	0.9751	1.0000
Total	100.00	100.00				

Fig. 9 Energy dispersive X-ray spectra (EDXS) on the fracture surface of the sintered at 1,120 °C

sizes are required along with full density. At this aim, further work is currently underway to obtain metastable solid solution, which helps in forming nanocomposites, by a more prolonged heavy mechanical milling of powders. In addition, the sintering process should be improved and the use of Spark Plasma Sintering could help to obtain fully consolidated specimens at low temperature with a slight increase of grain size. At this regard, new experiments are in progress and the results will be presented elsewhere.

Acknowledgments Mr. Victor Micheli is greatly acknowledged for the hardness measurements.

References

1. Ma E (2000) Powder Metall 43:306
2. German RM (1984) Powder injection moulding. Metal Powder Industries Federation, Princeton, New Jersey
3. Wang JS, Lin SP, Hon MH, Wang MC (2000) Jpn J Appl Phys 39:616
4. Di Maggio R, Gialanella S, Cesconi M, Molinari A (2003) Mater Sci Technol 19:1585
5. Di Maggio R, Fambri L, Guerriero A (1998) Chem Mater 10:1777
6. Di Maggio R, Fambri L, Cesconi M, Vaona W (2002) Macromolecules 35:5342
7. Lenel FV, Hwang KS (1980) Powder Metall Int 12:581
8. Lenel FV (1980) Powder metallurgy: principle and application. Metal Powder Industries Federation, Princeton, NJ, p 285
9. Wanible Y, Yokoyama H, Itoh T (1990) Powder Metall 33:65
10. Huang CT, Hwang KS (1996) Powder Metall 39:119
11. Lawlock RL, Davies TJ (1990) Powder Metall 33:147
12. Shen P, Hu JD, Guo ZX, Guan QF (1999) Metall Mater Trans 30A:2229
13. Holtz RL, Provenzano V (1994) Nanostruct Mater 4:241
14. He L, Ma E (1996) Nanostruct Mater 7:327 and references therein
15. He L, Ma E (1996) J Mater Res 11:72
16. Lutterotti L, Matthies S, Wenk H-R (1999) IUCr. Newsletter of the CPD 21:14
17. Deletz R (1993) In: Young RA (ed) The Rietveld method. IUCR monographs on crystallography
18. Oliver WC, Pharr GM (1992) J Mater Res 7:1564
19. Oliver WC, Pharr GM (2004) J Mater Res 19:3
20. Ma E, Atzmon M, Pinkerton FE (1993) J Appl Phys 74:955
21. Lábár JL (2002) Microscopy and analysis 75:9
22. Huang Z, Gu LY, Weertman JR (1997) Scripta Materialia 37:1071
23. Yamaguchi K, Takakura N, Imatani S (1997) J Mater Proc Technol 63:364
24. Radchenko OG, Getman OI (2001) Int J Hydr Energy 26:489
25. Entel P, Kreth M, Meyer R, Kadau K (2004) Proceedings of the 3rd international conference on computational modeling and simulation of materials. In: Vincenzini P, Zerbetto F (eds) Advances in science and technology, vol 44. Acireale Italy, Techna Group, pp 101–112
26. Lee GH, Rhee CK, Lee MK, Kim WW, Ivanov VV (2004) Mater Sci Eng A 375–377:604